PNAS Nexus, 2023, 2, 1–12
https://doi.org/10.1093/pnasnexus/pgad269
Advance access publication 17 August 2023
Research Report

Membrane free-energy landscapes derived from atomistic dynamics explain nonuniversal cholesterol-induced stiffening

Giacomo Fiorin [a,b,*], Lucy R. Forrest [a,*] and José D. Faraldo-Gómez [b,*]

[a]National Institute for Neurological Disorders and Stroke, Bethesda, MD 20892, USA
[b]National Heart, Lung and Blood Institute, Bethesda, MD 20894, USA
*To whom correspondence should be addressed: Email: giacomo.fiorin@nih.gov; lucy.forrest@nih.gov; jose.faraldo@nih.gov
Edited By: Dennis Discher

Abstract

All lipid membranes have inherent morphological preferences and resist deformation. Yet adaptations in membrane shape can and do occur at multiple length scales. While this plasticity is crucial for cellular physiology, the factors controlling the morphological energetics of lipid bilayers and the dominant mechanisms of membrane remodeling remain to be fully understood. An ongoing debate regarding the universality of the stiffening effect of cholesterol underscores the challenges facing this field, both experimentally and theoretically, even for simple lipid mixtures. On the computational side, we have argued that enhanced-sampling all-atom molecular dynamics simulations are uniquely suited for the quantification of membrane conformational energetics, as they minimize a priori assumptions and permit analysis of bilayers in deformed states. To showcase this approach, we examine reported inconsistencies between alternative experimental measurements of bending moduli for cholesterol-enriched membranes. Specifically, we analyze lipid bilayers with different chain saturation and compute free-energy landscapes for curvature deformations distributed over areas from ∼5 to ∼60 nm^2. These enhanced simulations, totaling over 100 μs of sampling time, enable us to directly quantify both bending and tilt moduli and to dissect the contributing factors and molecular mechanisms of curvature generation at each length scale. Our results show that the effects of cholesterol on bending rigidity are lipid-specific and suggest that this specificity arises from differences in the torsional dynamics of the acyl chains. In summary, we demonstrate that quantitative relationships can now be established between lipid structure and bending energetics, paving the way for addressing open fundamental questions in cell membrane mechanics.

Keywords: biomembrane mechanics, cholesterol, free energy, molecular dynamics

Significance Statement

Elucidating the energetics and mechanisms of membrane remodeling is an important step towards understanding cell physiology. This problem is challenging, however, because membrane bending involves both large-scale and atomic-level dynamics, which are difficult to measure simultaneously. A recent controversy regarding the stiffening effect of cholesterol, which is ubiquitous in animal cells, illustrates this challenge. We show how a recently developed molecular-dynamics simulation method can bridge this length-scale gap and reconcile for example, how some cholesterol-rich membranes exhibit higher stiffness against stretching but not against bending deformations. This approach facilitates a conceptual connection between lipid chemistry and membrane mechanics, thereby providing a solid basis for future research on remodeling phenomena, such as in membrane trafficking or viral infection.

Introduction

All biological membranes resist deformations of their intrinsic shape. A membrane-bound protein may however reshape the surrounding bilayer, sometimes strikingly (1–8), because the free-energy cost of membrane bending can be offset by free-energy gains resulting from adequate solvation of the protein surface. In other words, lipid bilayers change shape around proteins to avoid large energetic penalties due to dehydration of ionized surface residues and/or exposure of large hydrophobic clusters to water. This kind of balance between competing energetic contributions is not uncommon and governs many other processes in molecular membrane physiology, including ligand-induced allostery, ion permeation, and so on. However, while atomic-resolution perspectives have become the state-of-the-art in experimental and theoretical analyses of protein structural dynamics, molecular recognition, or solvation energetics, the membrane is still often conceptualized assuming a continuous homogeneous medium. While insightful in some cases (9–13), the shortcomings of this perspective become quickly apparent for mixed-lipid bilayers, which are the norm in biological cells (14). And so, deceptively simple fundamental questions, such

Competing Interest: The authors declare no competing interest.
Received: March 14, 2023. **Revised:** July 31, 2023. **Accepted:** August 3, 2023

as how the chemical makeup of a bilayer dictates its intrinsic bending energetics, remain largely unresolved.

A recent controversy regarding the stiffening effect of cholesterol illustrates this challenge (15–17). Cholesterol is enriched in animal cell membranes and is known to dampen the dynamics of the surrounding lipids (18, 19) (Fig. 8), resulting in higher density, viscosity, and area elastic modulus K_A compared to cholesterol-free membranes. Because those effects apply to all lipid types, cholesterol was initially thought to universally enhance the bending rigidity k_c of all membranes as well. If so, generating curvature in cellular membranes would be more costly than in the synthetic bilayers often examined in laboratory conditions, and potentially entail distinct mechanisms. However, while analysis of bilayers of partially or fully saturated lipids confirmed the expected stiffening effect of cholesterol (20, 21), little or no effect was observed for unsaturated lipids like DOPC, when examined either with X-ray diffraction (21), tube aspiration (22, 23), or electrodeformation (24). This lipid-type specificity would have very interesting biological implications. For example, unsaturated lipids might localize at the periphery of domains enriched in saturated lipids (25) to mitigate the stiffening effect of cholesterol and help preserve the membrane's plasticity wherever needed. While appealing, however, this lipid-type specificity has been recently disputed by a study of microscopic membrane fluctuations based on neutron-spin echo (NSE), nuclear magnetic resonance (NMR) and conventional molecular dynamics (MD) simulations (15). In stark contrast to the preceding studies (21–24), this analysis concluded that the stiffening effect of cholesterol on bending energetics is likely universal for all lipid bilayers, including DOPC, and this notion quickly became the subject of debate (16, 17).

A possible complicating factor in this controversy is the need to rely on inference through continuum mathematical models, especially when performing measurements at "molecular" length scales of a few nanometers. However, that limitation can be circumvented by quantifying directly the structure and dynamics of lipid bilayers subject to an actual morphological perturbation. In this work, we showcase an advanced all-atom molecular simulation methodology that we recently developed (26) to address this kind of challenge. This methodology, which we refer to as "Multi-Map" sampling, provides a means to directly quantify free-energies of bending for lipid bilayers (5) and can be applied to bilayers of any chemical makeup, including model synthetic bilayers with or without cholesterol (26). This method differs from conventional simulation methods in that it mimics the action of proteins or laboratory manipulations that sustain curvature over long timescales, while providing atomically resolved insights into the structure and dynamics of the membrane as it is deformed. Our results support the notion that the stiffening effect of cholesterol on bending energetics is nonuniversal, and that it is specifically dependent on the degree of lipid-chain unsaturation. A mechanism is also proposed by which lipid unsaturation preserves flexibility despite the increased density and molecular order that cholesterol invariably induces. These insights permit us to rationalize, for example, how cholesterol affects stretching and bending deformations differently, by universally stiffening the former but not the latter. In conclusion, we posit that this emerging computational methodology, in combination with suitable experimental approaches, will facilitate a clearer understanding of the molecular mechanisms by which cells and organelles shape the morphology of lipid membranes.

Results

Bending free-energy profiles show cholesterol effects are lipid-type specific

Atomistic models of hydrated bilayers were prepared for the following compositions: pure POPC, pure DOPC, and 70:30 mixtures of either POPC or DOPC with cholesterol (CHOL), hereafter indicated as POPC/CHOL and DOPC/CHOL (Fig. 1). POPC and DOPC lipids were chosen because they have very similar bending moduli and radii of preferred curvature (27, 28). A 30% cholesterol mole fraction represents typical concentrations in eukaryotic membranes (29) and approaches the highest concentration that is still soluble in physiological phospholipids (30, 31). This concentration has also been shown to induce significant changes in molecular properties (15) and membrane mechanics (20, 21). For each bilayer, the same composition was used in both leaflets.

In order to examine deformations in curvature over different length scales, bilayers of 200, 800 and 1800 lipid molecules per periodic unit cell were prepared for each lipid composition, for a total of 12 membrane models. Respectively, the in-plane dimensions of these molecular systems are approximately 80×80, 160×160 and 240×240 Å^2 for the pure bilayers, and 70×70, 140×140, and 210×210 Å^2 for the mixed bilayers. All bilayers were simulated in atomistic detail and with explicit solvent at room temperature and pressure using two different sampling methods, generating in each case trajectories of multiple microseconds (Table 1).

In one approach, we simulated the bilayers at rest, without applying any extrinsic forces, to examine their spontaneous fluctuations. As will be discussed below, this analysis led to similar conclusions as in published work regarding the ordering of membranes by cholesterol, namely that the molecular order of the lipid bilayer is increased to a similar extent for both POPC and DOPC (Figs. 1 and 8). However, these simulations of bilayers at rest cannot directly reveal the energetics of bending. Instead, bending moduli k_c were extracted by analyzing membrane bending fluctuations using a continuum theory (32, 33). This analysis confirmed cholesterol's stiffening effect on POPC, but it was inconclusive for DOPC due to the inherent statistical uncertainty (Fig. 7 and Table S1).

To more directly evaluate the effect of cholesterol on the energetics of membrane bending, we used the Multi-Map enhanced-sampling method (26). In this approach, the membrane is subject to increasingly large deformations whose energetic cost is computed directly, i.e. without requiring the use of a continuum theory. This task is achieved by defining a collective variable (or reaction coordinate) that reflects the membrane shape and

Table 1. Simulations of all-atom lipid bilayers carried out in this work.

Composition	Conventional MD sampling time (single replica), μs			Multi-Map enhanced MD sampling time (replica count × time), μs		
POPC	5.3	5.9	3.3	13 × 0.3	12 × 0.6	12 × 1.5
POPC/CHOL	8.9	9.1	3.4	13 × 0.7	14 × 0.7	13 × 1.5
DOPC	2.0	6.5	3.3	15 × 0.1	14 × 0.7	13 × 1.5
DOPC/CHOL	6.2	7.5	3.4	12 × 0.7	15 × 0.6	13 × 1.5
Number of lipids per unit cell	1800	800	200	1800	800	200

The calculations based on enhanced-sampling Multi-Map simulations entailed multiple replicas with increasing degrees of applied curvature, carried out in parallel.

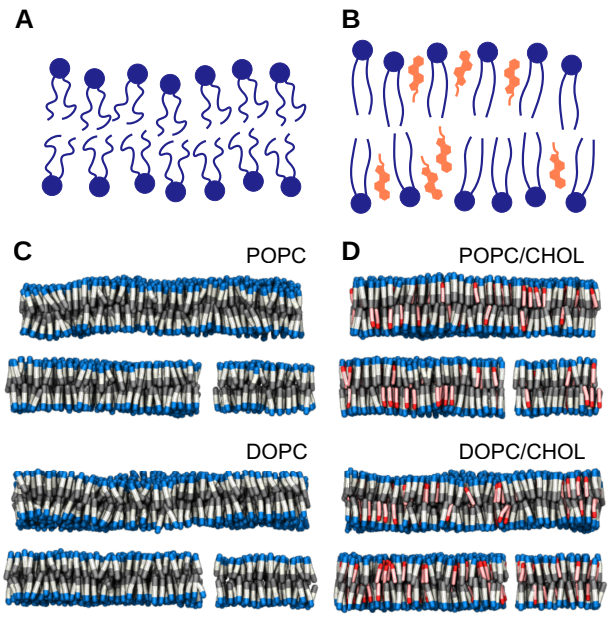

Fig. 1. Cholesterol-enriched bilayers. A,B) Schematic of the effect of cholesterol on lipid membrane order. C) Snapshots from all-atom simulations of pure-POPC and pure-DOPC bilayers at rest; lipid molecules are visualized as rods. The water buffer is omitted for clarity. D) Simulation snapshots of POPC/CHOL and DOPC/CHOL bilayers. Phospholipid and cholesterol molecules are represented as rods and smaller rods, respectively.

curvature (26) and by forcing this variable to explore values well beyond its thermal fluctuations through a series of progressively shifted biasing potentials following the umbrella-sampling protocol (34). Here, the bilayers were driven to adopt a periodic sinusoidal shape along the x-axis, gradually varying the amplitude of the sinusoid to induce greater curvature. It is important to note that while each biasing potential fosters an average shape for the membrane midplane, it does not influence its fluctuations around that shape, nor does it impose one or other mechanism of bending at the molecular level. By collecting the probability distribution of different bilayer states, we then derived for each bilayer the potential of mean force (PMF), or free-energy profile, as a function of the applied curvature c.

These PMF profiles, shown in Fig. 2, clearly demonstrate that bending a POPC/CHOL bilayer is significantly more costly than bending a POPC bilayer, for curvature deformations of comparable shape and length-scale (Fig. 2). That is, cholesterol has a substantial stiffening effect on POPC membranes. By contrast, the free-energy curves for DOPC and DOPC/CHOL are nearly identical (Fig. 2), i.e. cholesterol has a minimal influence on the plasticity of the DOPC membranes, despite its effect on molecular order.

It is worth noting that the statistical error of the PMF profiles shown in Fig. 2 is very small, despite the large computational cost of the calculations; that is, these curves are faithful representations of the free-energy cost of membrane bending at the corresponding length scale, given the forcefield used in the simulations. This precision results from extensive configurational sampling; e.g. for DOPC and DOPC/CHOL, the total sampling times employed in the PMF calculations are an order of magnitude longer than those in early applications of the Multi-Map method (26). The current results, therefore, supersede previous data for these bilayers.

Based on the above data alone, and in the absence of fitting to a continuum model, it can be concluded that the stiffening effect of cholesterol on bending energetics is lipid-type specific rather than universal. Nonetheless, to enable direct comparison with other experimental and computational approaches, it is useful to also quantify this stiffening effect by estimating the associated bending modulus k_c. Derivation of k_c, however, requires further analysis of our curved-membrane trajectories, because the dominant mechanisms of bending depend on the length scale of the curvature deformation at the molecular level (32, 33, 35, 36). This problem is addressed in the next section.

Determination of bending and tilt moduli from analysis of curved lipid bilayers

The Helfrich–Canham theory (37, 38) idealizes the lipid bilayer as a homogeneous, harmonic elastic medium represented by its midplane. The free-energy density of bending this membrane, f_{HC}, relies on a single parameter, the bending modulus k_c, and has the following expression:

$$f_{HC}[h] = \frac{1}{2} k_c (\nabla \cdot \mathbf{N})^2 \quad (1)$$

where $h(x, y)$ is a two-dimensional function that maps the difference between the shape of the deformed bilayer and a flat shape. f_{HC} depends directly on the second derivatives of h, or equivalently the first derivatives of the vector perpendicular to the membrane midplane $\mathbf{N} = (\partial_x h, \partial_y h, -1)$, save for normalization. The Helfrich–Canham model therefore implicitly assumes a mechanism wherein, on average, all lipid molecules remain parallel to the normal vector $\mathbf{N}$, and therefore bending entails deflections in the relative orientations of adjacent lipid molecules (Fig. 3A).

While this assumption is plausible for deformations occurring over "macroscopic" length-scales, it is increasingly recognized that the average lipid orientation in more localized bending is not solely described by the shape of the membrane midplane; that is, lipids can "tilt" relative to the normal vector $\mathbf{N}$ (Fig. 3B). A more general free-energy functional is therefore the following (32, 33):

$$f_{HK}[h, \mathbf{n}] = \frac{1}{2} k_c (\nabla \cdot \mathbf{n})^2 + \frac{1}{2} k_t |\mathbf{n} - \mathbf{N}|^2 \quad (2)$$

where $\mathbf{n}$ maps the lipid orientation across the membrane and k_t is referred to as the lipid-tilt modulus. Note that while the first term in Eq. 2 is very similar to Eq. 1, $\mathbf{n}$ varies more smoothly than $\mathbf{N}$ at short length scales (<100 Å, Fig. 3B) and thus the free-energy cost of bending according to Eq. 2 can be significantly smaller than that predicted by the Helfrich–Canham model (Eq. 1). The spectral density of the bending fluctuations predicted by Eq. 2 has been supported by many MD simulations and experiments (28, 39–42). Furthermore, Eq. 2 was also validated by showing that the fluctuations of the membrane midplane and those of the lipid tilt vector ($\mathbf{n} - \mathbf{N}$) are described by the same moduli k_c and k_t (35, 43).

The above theory is transferable over a wide range of length scales ($L \geq 30$ Å) and can be used to derive k_c and k_t from spontaneous fluctuations of a membrane at rest, either by simulation or experiment. However, because membrane fluctuations are transient, $\mathbf{n}$ and $\mathbf{N}$ are difficult to resolve in both position and time, requiring substantial averaging. This challenge is greater when the intrinsic bilayer shape is flat, as $\mathbf{n}$ and $\mathbf{N}$ fluctuate around the same fixed direction, and only their fluctuations carry physical information. By contrast, evaluation of $\mathbf{n}$ and $\mathbf{N}$ can be more informative if the membrane is examined under applied curvature, as each element varies very significantly across the bilayer, to an extent that can be predicted by Eq. 2.

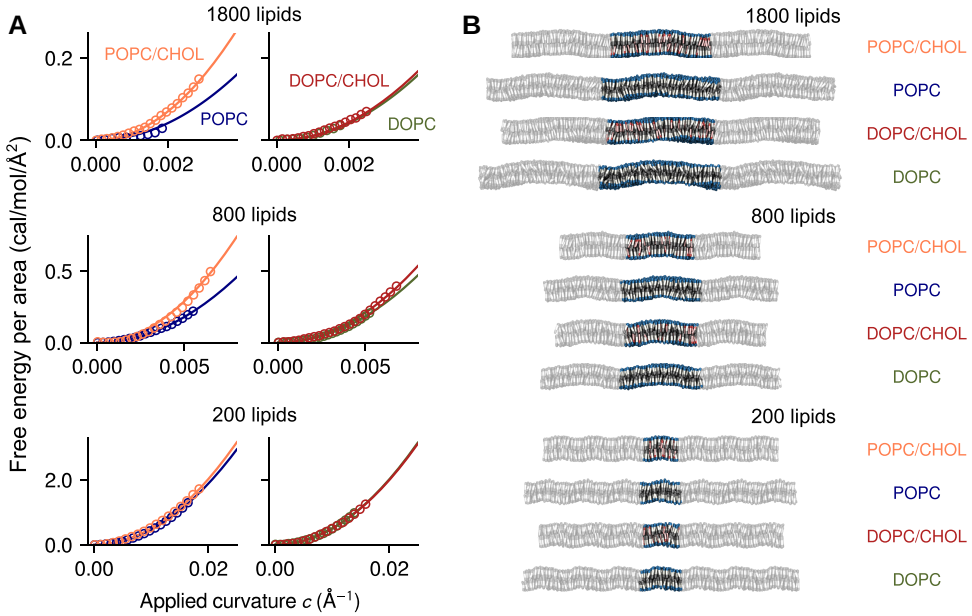

Fig. 2. Direct calculation of the free-energy cost of lipid bilayer bending using the Multi-Map enhanced-sampling simulation method. A) Potentials-of-mean-force (PMFs) as a function of the applied bilayer curvature c for an applied sinusoidal shape along the x-axis; using c as abscissa facilitates direct comparisons between bilayers of different sizes (in contrast to e.g. the peak amplitude of the deformation (26)). Data are shown for POPC, POPC/CHOL, DOPC, and DOPC/CHOL bilayers, containing either 1800, 800 or 200 lipid molecules (as indicated). All PMF profiles are given in units of free-energy per area; symbols indicate computed values and solid lines are quadratic fits assuming PMF = Bc^2, where the fit error on B is ≤0.2 kcal/mol. B) Representative snapshots of each bilayer, represented in Fig. 1. The figure highlights the periodic unit cell, flanked by its images along the direction of the sinusoid.

For example, for a periodic sinusoidal shape along the x-axis, it is straightforward to evaluate the three components of **N** and their derivatives at any point along the bilayer, and its only longitudinal component is N_x, hereafter labeled as $N_\parallel$. By minimizing Eq. 2 with respect to the corresponding orientation component, $n_\parallel$, we obtain the following expression:

$$\frac{n_\parallel}{N_\parallel} = \left(1 + \frac{k_c q^2}{k_t}\right)^{-1} \tag{3}$$

where $q = 2\pi/L$ and L is the length of the sinusoidal curvature deformation (i.e. the bilayer size). Note that because $N_\parallel$ and $n_\parallel$ are constant along the y axis, the "twist" term $\nabla \times (\mathbf{n} - \mathbf{N})$ (32, 35, 42) can be safely neglected and thus was not included here for clarity. Splay-tilt coupling (44) was similarly neglected because it is thought to be significant only at very high q (42).

Based on the same trajectory data used for the derivation of the PMF curves (Fig. 2) we calculated the ratio $n_\parallel/N_\parallel$ for each bilayer using linear regression (Fig. S1), consistent with the underlying assumption of linear response (32). For pure POPC and DOPC, we find that the simulation data and Eq. 3 are in excellent agreement when using known values of k_c/k_t (27) without any additional fitting (Fig. 3D and E). This is a nontrivial result that confirms our methodology based on analysis of extrinsically curved bilayers is sound. We thus proceeded to determine k_c and k_t for POPC/CHOL and DOPC/CHOL membranes, which to our knowledge had not been previously estimated. We again find that Eq. 3 also describes our data very well for these mixtures, using the k_c/k_t ratio as the only fitting parameter (Fig. S2).

This strategy of mapping the tilt of individual lipids relative to the membrane plane enabled us to derive bending moduli k_c and tilt moduli k_t for each lipid composition, as shown in Fig. 4 and Table 2. Pure POPC and pure DOPC exhibit very similar moduli, with the former exhibiting a slightly higher k_c albeit within statistical error, as shown previously (27, 28). When comparing POPC and POPC/CHOL bilayers, we find that k_c increases by a factor of 2.1 ± 0.2 (Fig. 4A), confirming that cholesterol has a significant stiffening effect for this type of lipid. Our estimate is in excellent agreement with k_c values obtained from tube-aspiration measurements, which yield a 2.3-fold increase (20). By contrast, the relative change in k_c between DOPC and DOPC/CHOL is 1.1 ± 0.1 (Fig. 4B), consistent with multiple measurements that indicate no stiffening (21–24). Although those experiments probed "macroscopic" length-scales, our results now show that the effect of cholesterol on DOPC is also minimal at length scales comparable to the membrane thickness ($L < 100$ Å). Indeed, the effect of cholesterol on this scale is also small for POPC (see the 200-lipid system, Fig. 2A, as tilting becomes more dominant, thereby mitigating the free-energy cost of curvature, Fig. 3D).

In summary, our simulation data show that the stiffening effect of cholesterol on bending energetics is lipid-composition dependent, i.e. nonuniversal. More specifically, stiffening is very pronounced for POPC but marginal for an unsaturated lipid-like DOPC. It is worth noting that the effect of cholesterol on POPC bilayers can also be small, but only if the deformations are very localized. At larger length scales, however, cholesterol causes POPC and DOPC bilayers to have a very different plasticity.

Rotational dynamics around unsaturated bonds appears to explain differential cholesterol effect

Although Eq. 2 may be used to calculate the free energy of membrane bending when empirical parameters such as k_c and k_t are known or assumed, no continuum theory can explain how these parameters depend (or not) on the lipid composition of the membrane. This explanation requires examining the internal molecular structure and dynamics of curved bilayers and the precise configuration of their constituent lipids. To that end, we used

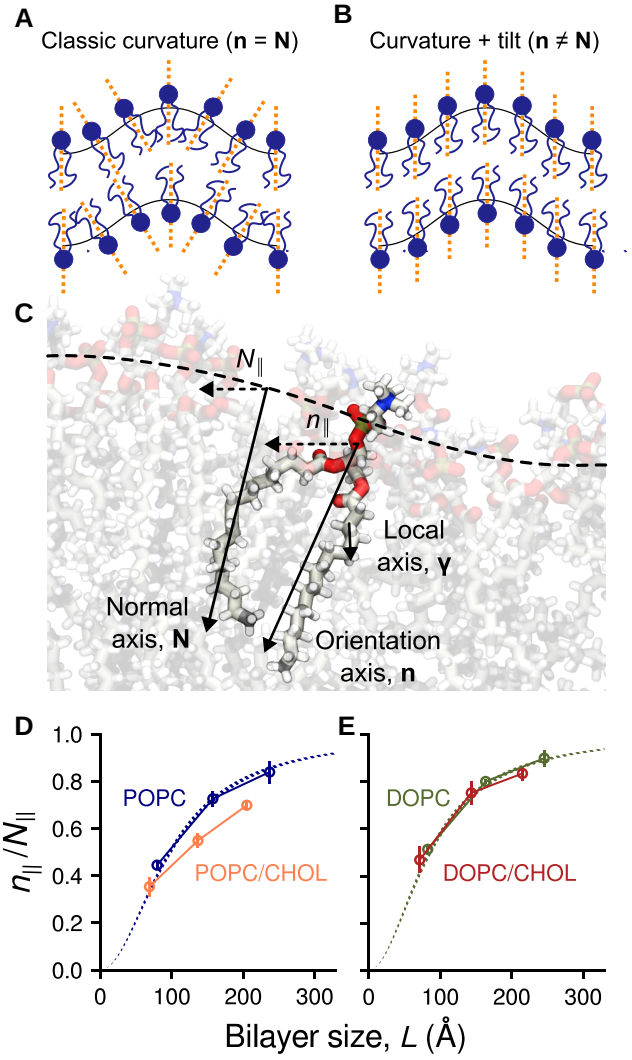

Fig. 3. Membrane bending entails midplane curvature and lipid tilt. A,B) Schematic of an idealized curved bilayer wherein one or other term of Eq. 2 (32) dominates the energetics. C) Illustration of the membrane normal vector, **N**, the lipid orientation vector (or lipid director), **n**, and the local chain vector **γ**, analyzed in Fig. 6. The ratio $n_{\parallel}/N_{\parallel}$ measures the degree to which midplane curvature defines the bending energetics; $n_{\parallel}/N_{\parallel} = 1$ only in the "macroscopic" limit, where the Helfrich–Canham model is valid. D,E) Mean values of $n_{\parallel}/N_{\parallel}$ for POPC, POPC/CHOL, DOPC and DOPC/CHOL, calculated from the same MD trajectories used to derive the PMF profiles in Fig. 2. Error bars represent standard errors. Dashed lines show the theoretical predictions for DOPC and POPC using Eq. 3 and published values of k_c/k_t (27).

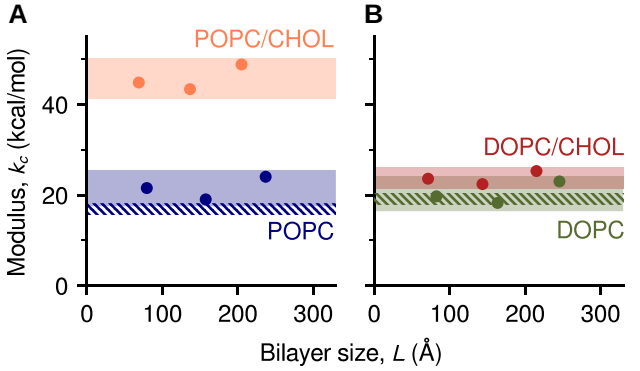

Fig. 4. The stiffening effect of cholesterol is lipid-type specific. Calculated bending moduli k_c are plotted as a function of bilayer size for different bilayers of A) POPC and POPC/CHOL, and B) DOPC and DOPC/CHOL. All values were derived from the analysis of MD trajectories of curved bilayers, by deriving the values of k_t/k_t for each composition from fitting $n_{\parallel}/N_{\parallel}$ against Eq. 3, and then using those values to fit the computed PMFs against Eq. 2 to derive k_c and k_t simultaneously. Shaded bands indicate the estimated 95% CI of k_c (Table 2), and dashed bands indicate the 95% CIs of k_c from tilt fluctuations of pure lipids (27).

our trajectory data to examine several plausible descriptors, namely membrane thickness and local cholesterol enrichment, as well as hydration of the hydrocarbon chains and their rotational freedom. All these properties fluctuate on time scales shorter than microseconds, and therefore our trajectories yield excellent statistics.

We observed no significant correlations between applied curvature and local bilayer thickness for either lipid type or length scale (Fig. 5A and B), ruling out local thickness as a reason for the differential effect of cholesterol. For bilayers with the more localized deformations ($L < 100$ Å), we observed a small increase in the local cholesterol concentration (<0.5 mol%) correlated with the regions where the membrane has the highest curvature ($c \approx 0.02$ Å^{-1}, Fig. 5C and D). However, this modest enrichment is similarly small for both POPC/CHOL and DOPC/CHOL. Therefore, local enrichment also does not explain either why cholesterol stiffens POPC but not DOPC (Fig. 2); instead, this enrichment likely reflects a general preference of cholesterol for concave curvatures. Recent MD simulation results, showing that local thickness affects cholesterol distribution much more strongly than curvature does (45), support the notion that local enrichment of cholesterol is more costly than typical bending deformations. Our analysis also ruled out the degree of hydration of the hydrocarbon chains as a differential factor; as expected, we found a clear correlation between curvature and water exposure of the acyl chains, but only for the pure-lipid bilayers and not for their cholesterol mixtures (Fig. S4).

A differential effect of cholesterol on DOPC and POPC bilayers was however revealed when examining the extent to which increasing curvature alters the orientational dynamics of individual acyl-chain segments. This analysis entails evaluation of the vectors formed by every pair of carbon atoms spaced by two chemical bonds in each lipid chain (Fig. 3C):

$$\boldsymbol{\gamma}(i) = (\mathbf{x}_{i+1} - \mathbf{x}_{i-1}) \quad (4)$$

Similar to the analysis of lipid molecule orientation associated with Eq. 3, the longitudinal component of the acyl-chain bond vectors, $\gamma_{\parallel}(i)$ (Fig. 3C), was evaluated and the ratio $\gamma_{\parallel}(i)/N_{\parallel}$ was quantified through regression. The result was then normalized against the relative orientation of the entire lipid ($n_{\parallel}/N_{\parallel}$), to quantify the dynamics of the ith segment relative to other segments in the same lipid molecule. Therefore, a rigid molecule would be described by the identity $\gamma_{\parallel}(i) = n_{\parallel}$, whereas in a flexible molecule, a higher value of $\gamma_{\parallel}(i)/n_{\parallel}$ indicates a greater deflection of that particular chain segment in response to bilayer curvature.

The results of this analysis are shown in Fig. 6 for the 200-lipid bilayers and in Fig. S7 for all bilayers. In the absence of cholesterol, the relative magnitude of reorientation $\gamma_{\parallel}(i)/n_{\parallel}$ is highest for the chain segments that are most proximal to the head groups ($i < 3$) and decays rapidly over a distance shorter than the chain persistence length (≈6 Å), reaching a minimum near the center of each chain. Cholesterol lowers the value of $\gamma_{\parallel}(i)/n_{\parallel}$ even further, with the largest effects observed in the saturated *sn*-1 chain of POPC

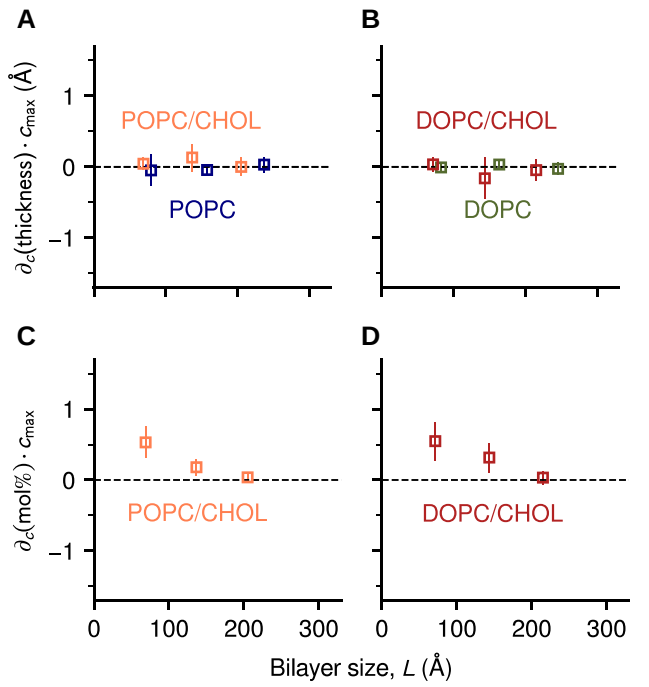

Fig. 5. Differential stiffening effect is not explained by curvature-induced variations in bilayer thickness or local cholesterol enrichment. A,B) Derivatives of the thickness with respect to curvature for different bilayers of A) POPC and POPC/CHOL, or B) DOPC and DOPC/CHOL. The derivatives were estimated by linear regression of the thickness map $t(x, y)$ against the curvature map of the midplane, $c(x, y)$. C,D) Derivatives of the cholesterol concentration with respect to curvature for different bilayers of C) POPC/CHOL and DOPC/CHOL, estimated by linear regression of the 2D histograms of cholesterol on each leaflet against $c(x, y)$ and $-c(x, y)$, respectively. For ease of comparison, the resulting slopes were multiplied by the largest applied curvature c_{max}; error bars represent standard errors.

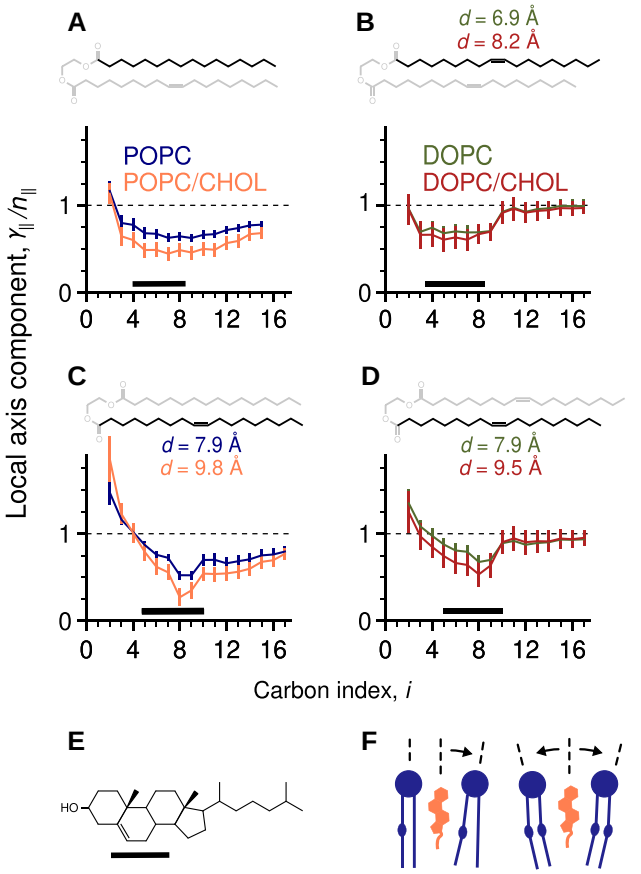

Fig. 6. Location of unsaturated bonds relative to cholesterol explains lack of stiffening effect on DOPC. Shown are mean values, computed over independent simulations of curved 200-lipid bilayers, of the ratio between the longitudinal components of the local chain axis orientation vector, $\gamma_{\parallel}$, and of the lipid orientation vector $n_{\parallel}$; error bars are standard deviations. A) Values for the *sn*-1 chains in POPC and POPC/CHOL bilayers, and B) in DOPC and DOPC/CHOL bilayers. C,D) Equivalent results for the *sn*-2 chains in the same bilayers. Above each panel, the chemical structure of the acyl chain is highlighted, with text labels reporting the mean distance d of each unsaturated bond from the midplane (standard deviations are ≃5 Å). Thick horizontal bars indicate the central 50% of the density of the sterol group, also drawn in E) for reference. F) Illustration showing how ordered saturated chains hinder curvature generation compared to ordered unsaturated chains; dashed lines indicate the lipid orientation vector **n**.

(Fig. 6A), and near the sterol group in general ($4 \le i \le 10$). It is outside of this region, however, that DOPC and POPC respond to curvature deformations in entirely different ways, which in turn explains the distinct effect of cholesterol.

In DOPC, segments between the third and the ninth carbon in each chain exhibit a smaller deflection than the lipid molecule as a whole ($\gamma_{\parallel}(i) < n_{\parallel}$), whereas the segments beyond the ninth carbon pivot relatively freely, manifested as $\gamma_{\parallel}(i) \sim n_{\parallel}$ (Fig. 6B and D). The inflection point between the two regions coincides with the location of the unsaturated bonds between the ninth and tenth carbon atoms. For comparison, the neutral plane of bending fluctuations of DOPC monolayers had previously been located slightly above the unsaturated bonds, i.e. ∼9.4 Å from the bilayer midplane (27). This location of the neutral plane is thus consistent with a bending mechanism where most of the reorientation of DOPC molecules is generated by the deflection of segments near the head groups ($i < 3$) or below the unsaturated bonds ($9 < i < 18$). Strikingly, cholesterol only appears to slightly restrain the deflection of the former without significantly affecting the latter (Fig. 6B and D), thus preserving both the underlying mechanism of reorientation of the DOPC molecules and its magnitude.

The rotational dynamics of each chain segment is significantly different for POPC. Although the unsaturated *sn*-2 chain exhibits some flexibility near the ninth carbon, as observed for DOPC, $\gamma_{\parallel}(i) < n_{\parallel}$ for most segments of the unsaturated *sn*-2 chain (Fig. 6C) and of the saturated *sn*-1 chain (Fig. 6A). Therefore, although the neutral planes of POPC and DOPC have very similar locations (27), it is not possible for POPC to identify regions of significantly higher or lower flexibility besides the headgroup itself. This fact alone might suggest that pure POPC may feature a higher k_c than pure DOPC, but the shorter 16-carbon *sn*-1 chain in POPC might imply the opposite; unsurprisingly, the two pure-lipid k_c values estimated here are comparable within error (Table S1). When cholesterol is added to POPC, the flexibility of most chain segments decreases further (Fig. 6A and C), consistent with a limited ability of the POPC molecule to comply with applied bilayer curvature, i.e. with a higher bending modulus k_c.

Analysis of spontaneous fluctuations of membranes at rest is inconclusive

In the preceding sections, we have shown how specialized MD simulations designed to induce steady-state curvature deformations in membranes can be used not only to quantify their bending energetics and empirical parameters often used in analytical theories but also to pinpoint the molecular origins of observed

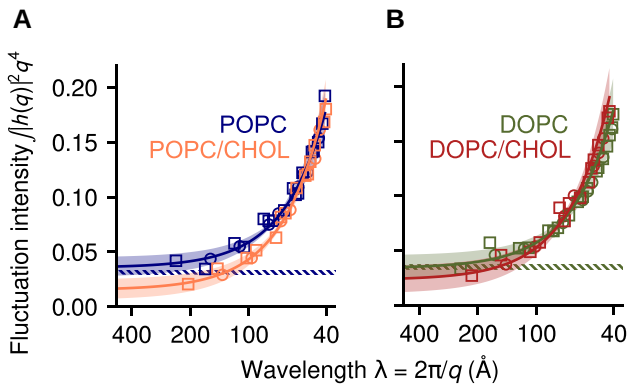

Fig. 7. Spectral analysis of bending fluctuations of bilayers at rest, based on conventional MD simulations. Only the 800- and 1800-lipid bilayers in Table 1 were considered (and analyzed together), as the 200-lipid bilayers do not sample adequately the first term of Eq. 5. A) POPC and POPC/CHOL bilayers (**$P = 0.002$). B) DOPC and DOPC/CHOL bilayers ($P = 0.24$). Solid lines are best fits of the function in Eq. 5, with shaded bands indicating the 95% confidence interval (CI). *P*-values are for comparisons of k_c with and without cholesterol. For comparison, dashed bands show the 95% CI for POPC and DOPC under the q^{-4} long-wavelength Helfrich–Canham theory (37, 38), using published values of k_c (27).

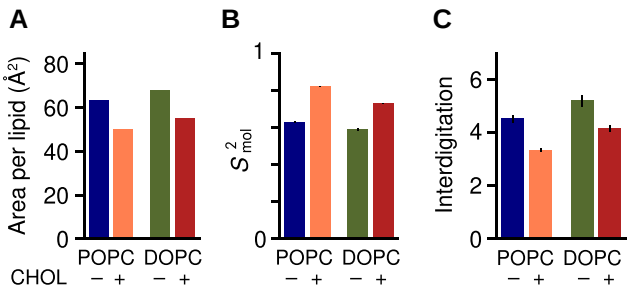

Fig. 8. Nonspecific cholesterol effects on membrane order and structure, irrespective of lipid-chain saturation. A) Area per phospholipid molecule computed for bilayers of POPC, POPC/CHOL, DOPC and DOPC/CHOL. B) Orientational order parameter S^2_{mol} of lipid molecules, for the same bilayers. C) Degree of entanglement between leaflets, estimated using the number of interdigitating acyl-chain bonds. All data were computed from simulations of bilayers at rest.

Table 2. Bending and tilt moduli for pure and mixed bilayers (means and 95% confidence intervals over the three bilayer sizes).

	k_c (kcal/mol)	k_t (kcal/mol/Å^2)
POPC	21.6 [17.6, 25.6]	0.104 [0.085, 0.124]
POPC/CHOL	45.7 [41.2, 50.2]	0.111 [0.100, 0.122]
DOPC	20.9 [17.1, 24.7]	0.114 [0.094, 0.134]
DOPC/CHOL	23.8 [21.5, 26.1]	0.134 [0.121, 0.147]

variations against lipid composition. Studies of lipid bilayers at rest using conventional MD simulations are however far more common; in this section, we show that while analysis of spontaneous fluctuations is certainly insightful, the information gained by this route is ultimately limited.

Specifically, for each of the lipid bilayer compositions considered above, now examined at rest, we calculated an MD trajectory spanning multiple microseconds (Table 1). We then quantified the spontaneous shape fluctuations of the membrane midplane for each trajectory snapshot by evaluating the instantaneous position of each lipid molecule (represented by its center of mass) relative to the bilayer center, i.e. $h(x_i, y_i) = (z_i - \langle z \rangle)$. The 2D Fourier transform of h, denoted by $h_{\mathbf{q}}$, was then computed over all wave vectors with wavenumber $|\mathbf{q}| < 0.2$ Å^{-1}, which is the appropriate limit for all-atom simulations (42). The resulting values of $|h_{\mathbf{q}}|^2$ were then averaged over all trajectory snapshots collected for $t > 0.5$ μs, and data points with equal $|\mathbf{q}|$ combined. To relate the calculated spectrum of bending fluctuations to the bending and tilt moduli, we used the following expression, based on Eq. 2 (28, 32, 35, 42):

$$\langle |h_{\mathbf{q}}|^2 \rangle = k_B T \left(\frac{1}{k_c q^4} + \frac{1}{k_t q^2} \right) \quad (5)$$

The results of this analysis are shown in Fig. 7 and Table S1. For both POPC and DOPC membranes, we find that bending and tilt moduli can be determined with reasonable certainty (15% error); our values of k_c agree well with estimates obtained with previous MD simulations or with "flicker" spectroscopy (27, 35), which are slightly smaller than those deduced from X-ray diffraction data (28). (This discrepancy has been discussed elsewhere and remains to be understood (27, 28): it has been speculated that the close spacing of the multilamellar stacks used for X-ray diffraction might introduce a favorable coupling between bilayers (27).) Overall, taking into consideration the different approximations and sources of error, experimental and computational methods indicate that POPC and DOPC bilayers have very similar k_c and k_t.

For POPC/CHOL and DOPC/CHOL, the statistical uncertainties are much higher (~35%, Table S1). As noted above, the fluctuations of the membrane midplane are much slower than those of individual lipid molecules and are further hindered when membrane viscosity is increased, as in the presence of cholesterol. Nonetheless, we can resolve a significant difference between the bending moduli k_c of POPC and POPC/CHOL (**$P = 0.002$; Fig. 7), consistent with the 2.3-fold increase measured by tube aspiration (20). However, it was not possible to detect statistically significant changes between DOPC and DOPC/CHOL; in the light of our direct analysis of bending energetics, little or no difference is indeed the expected result, but without that information, the uncertainty inherent to this type of fluctuation analysis would preclude a conclusive quantitative answer to the question at hand.

For completeness, we note that the spontaneous fluctuations of a membrane at rest might be examined differently; for example, a method has been reported that analyzes the fluctuations of the lipid-tilt field ($\mathbf{n} - \mathbf{N}$), which are uniquely accessible to MD simulation (35). (NMR also measures the fluctuations of $\mathbf{n}$, but they are aggregated with those of $\mathbf{N}$ as well as movements of individual atoms (46).) While this tilt-fluctuations analysis (35) can be more precise than the bending-fluctuations analysis (Eq. 5), the former has not yet been validated on mixed-composition bilayers and therefore we did not consider it here.

On the universality of other cholesterol effects

To conclude, it is worth clarifying that while cholesterol might not have a strong influence on the bending energetics of bilayers of a certain lipid-type, some effects do appear to be universal. For example, there is consensus that when cholesterol is mixed with any kind of phospholipids, it significantly dampens their motion and increases their alignment with the membrane normal, as illustrated in Fig. 1B. Both effects are indeed observed in our simulations of membranes at rest, and translate into clear differences in the area per lipid molecule (Fig. 8A) and in the atomic order parameters upon addition of cholesterol to both lipid types (Fig. S5). Consistent with earlier analyses (47), the difference is higher for

saturated chains (*sn*-1 chain of POPC) than for unsaturated chains (DOPC and *sn*-2 chain of POPC).

An alternative metric of chain order that is independent of overall molecular orientation can be obtained by quantification of the rotational freedom of individual torsional angles, independent of overall molecular orientation (Fig. S6). This metric shows that adding cholesterol results in a significant loss of entropy per molecule for both POPC and DOPC, namely $-T\Delta S = 1.05$ and 0.44 kcal/mol, respectively (Fig. S6).

An additional route to quantify the orientational order of lipid molecules is through the auto-correlation function (ACF) of the lipid orientation vector:

$$\mathrm{ACF}_{\mathbf{n}}(t) = \langle P_2(\mathbf{n}_i(t_0) \cdot \mathbf{n}_i(t_0 + t)) \rangle_{t_0, i} \tag{6}$$

where $\mathbf{n}_i$ is the orientation vector of the ith lipid molecule, t_0 and t are time intervals, and $P_2(x) = (3x^2 - 1)/2$. Lipid orientation fluctuations are much faster than membrane curvature fluctuations (27, 35): therefore, Eq. 6 has a reasonably well-defined plateau near $t = 100$ ns, here indicated as S^2_{mol}. Cholesterol causes a significant increase in S^2_{mol} for both POPC and DOPC (Fig. 8B). We note that values of S^2_{mol} we obtain for DOPC and DOPC/CHOL (0.59 and 0.73, respectively) are in close agreement with those reported elsewhere (15).

We conclude this analysis by examining the area elastic modulus, K_A, which represents the energy gain associated with changes in the optimal area per lipid molecule at conditions of zero tension (as used throughout this work). Fig. S8 shows the values of K_A calculated from the area fluctuations along the simulated trajectories of the 200-lipid bilayers, whose area fluctuations are the least affected by spontaneous membrane bending. When averaging over independent simulations, the resulting values are: $K_A = 267 \pm 16$ mN/m (POPC), 529 ± 43 mN/m (POPC/CHOL), 299 ± 15 mN/m (DOPC) and 431 ± 25 mN/m (DOPC/CHOL). Therefore, although the magnitude of the effect differs, the increase in area modulus induced by cholesterol is substantial for both POPC and DOPC, consistent with the decreased flexibility and increased packing of the lipid molecules.

For bilayers that do not contain cholesterol, the polymer brush model (48) has often been used to relate the bending modulus k_c to the area modulus K_A and the hydrophobic thickness, measured as the spacing between polar head groups, d_{pp}:

$$k_c \simeq \beta K_A d_{pp}^2 \tag{7}$$

where the dimensionless constant β describes how bending strain propagates in the bilayer interior. Because the coupling between leaflets is challenging to quantify, an approximation is typically made by using $\beta = 1/24$, which is intermediate between the two limiting cases of a homogeneous monolayer with no midplane ($\beta = 1/12$) and two fully decoupled leaflets ($\beta = 1/48$). In principle, β should also account for the degree of lipid interdigitation (Fig. 8C): however, to our knowledge, no quantitative model currently exists for this property. Although the $\beta = 1/24$ approximation is reasonable for bilayers made of pure phospholipids due to their chemical similarity, it is not universally applicable to all bilayers (49).

Using area moduli K_A and thicknesses d_{pp} computed from the simulated trajectories (Figs. S3, S4 and S8), and assuming $\beta = 1/24$ as mentioned, Eq. 7 predicts that k_c increases by a factor of 2.6 ± 0.4 between POPC and POPC/CHOL. This estimate is consistent with experimental measurements (20) and other computations in this work, suggesting that a decrease in interdigitation (Fig. 8C) does not significantly affect bending stiffness as long as the two leaflets remain coupled. However, the predicted change between DOPC and DOPC/CHOL is 1.8 ± 0.2, which is far in excess of both experiments (21–24) and computation. Although, on the face of it, this analysis is consistent with the notion that CHOL universally stiffens the area compressibility K_A of both DOPC and POPC, using Eq. 7 with a fixed parameter $\beta = 1/24$ is not supported by the analysis of acyl chain mobility (Fig. 6). Specifically, in this context a POPC/CHOL bilayer might be idealized as two homogeneous leaflets bonded at the midplane, but DOPC/CHOL exhibits a discontinuous bending strain profile within each leaflet as well (Fig. 6B and D). Therefore, a unique parameter β is inadequate to represent this membrane, and by extension others of similar or greater complexity. Thus, this analysis further highlights the limited applicability of simplified models to study intricate membrane phenomena and underscores the need for detailed representations of the membrane structure and dynamics, such as the Multi-Map simulation approach adopted in the current study.

Discussion

To examine opposite claims in regard to the universality of cholesterol stiffening of lipid bilayers, resulting from distinct experimental approaches (16, 17), we used a recently developed simulation methodology (26) to compute bending free-energy curves for atomically detailed bilayers of POPC, DOPC and their mixtures with 30 mol% cholesterol, at length scales relevant in molecular physiology (50 to 250 Å). The results from this approach clearly show that while pure POPC and pure DOPC have very similar mechanical properties, and the addition of 30 mol% cholesterol has similar effects on certain mechanical properties (e.g. area elastic modulus K_A), the free-energies of membrane bending of POPC/CHOL and DOPC/CHOL are nonetheless very different. The Multi-Map simulation results are thus in line with a body of experimental evidence that supports the notion that the stiffening effect of cholesterol on bending rigidity is lipid-type specific, rather than universal (20–24). Most importantly, this conclusion was reached through direct quantification of the free energy of the membrane as a function of increasing curvature, forgoing the use of continuum mathematical models to approximate the relationship between them.

Because our computational methodology entails simulation of all-atom trajectories, it permits us to not only quantify the bending energetics of the membrane but also to inspect the underlying changes in its molecular structure. Lipid orientation was found to obey the energy functional described in Eq. 2 (32, 33), which had previously been shown to predict the magnitude of membrane bending fluctuations with excellent accuracy across a broad range of length scales (28, 39–42). In the context of this work, the joint analysis of membrane curvature and lipid orientation allowed the derivation of bending moduli k_c and tilt moduli k_t, whose values are conserved across bilayer sizes and consistent with independent studies on pure POPC and pure DOPC (27, 28).

When examined at the atomic level, POPC and DOPC were found to differ significantly in how they respond to applied curvature. Specifically, we observed that the unsaturated bonds allow both chains in DOPC to change orientation much more dynamically than the chains in POPC, and this effect is greatly amplified by cholesterol, owing to the precise location of these bonds relative to the preferred location of cholesterol in the membrane (Fig. 6). Interestingly, the location of the unsaturated bonds is highly conserved in mono-unsaturated lipid chains (47, 50), suggesting that our observations are transferable to other membranes containing

unsaturated lipids and might reflect an important biological function. It has been proposed that many mechanisms of intracellular trafficking rely on curvature-driven sorting of lipid species (see (51) and references therein). By amplifying differences in membrane stiffness with respect to lipid type, cholesterol might contribute to this sorting mechanism.

Our results for DOPC and DOPC/CHOL are at odds with recent studies that concluded that cholesterol universally stiffens all mechanical properties of the membrane, irrespective of lipid type (15, 52). The first study was based on the analysis of molecular-scale properties (area per lipid, thickness, atomic order parameters, lipid orientation) quantified by NMR and conventional MD simulations, as well as measurements of the relaxation rates of bending fluctuations from NSE. Bending moduli k_c were estimated based on the measurements of those techniques by using previously developed theoretical models (46, 53, 54). In the second study, k_c was inferred instead from the distribution of diameters of giant vesicles (52).

The studies above, as well as many others, share the commonly used approach of connecting the bending modulus k_c to a different property via theoretical models. That approach can be advantageous particularly at "molecular" length scales, because it circumvents the challenging task of directly measuring the free energy of membrane bending or the magnitude of its fluctuations. Furthermore, theoretical analysis and the inference of k_c are needed even when a technique reports directly the free-energy of membrane bending (Fig. 2), if only to compare with existing work. However, the results of each theoretical model ultimately reflect its underlying assumptions or approximations. This is exemplified by the polymer brush model (48), which aims to predict the energy cost of bending a membrane, i.e. k_c, based on the energy needed to stretch that membrane from its resting area, i.e. from K_A. As shown in the previous section, this type of model is based on physically measurable quantities, such as K_A or the membrane thickness, but also additional factors, such as β, which cannot be measured (48).

Similar considerations can apply to some of the models developed to interpret a specific type of measurement. For example, in Chakraborty et al. (15), k_c was inferred from NMR measurements by modeling the relative magnitude of "fast" and "slow" fluctuations through a single parameter $S_s = 0.6$ irrespective of the varying lipid composition (46). In the framework of this paper, that assumption would be equivalent to assuming that the ratio k_c/k_t is a universal constant, which is inconsistent with our findings even for membranes where stiffening is observed, e.g. between POPC and POPC/CHOL (Table 2).

Another example is in the analysis of the "splay" angle between pairs of neighboring lipid molecules based on conventional MD simulations of small bilayers (15, 54). This analysis is both informative and numerically reproducible (Fig. S10); however, theoretical inference of k_c from that analysis requires the additional approximation that lipid tilt and splay are decoupled from each other, i.e. that $\mathbf{n}$ and $(\nabla \cdot \mathbf{n})$ fluctuate independently (54).

Lastly, the dissipation rates of membrane bending fluctuations can be measured using NSE with nanometer-scale resolution. However, because the model currently used to analyze those rates entails multiple dissipation effects, a separation of time scales is typically assumed to allow the use of single-exponential decay functions (53). We tested that assumption on the simulated trajectories of bilayers at rest, observing that it applies well to pure POPC or pure DOPC, but not to POPC/CHOL or DOPC/CHOL (Fig. S9A to H). We emphasize that the latter finding only applies to the mechanism of dissipation because dynamic membrane properties such as viscosity or interleaflet friction (55) are universally increased by cholesterol. Further, this effect on viscosity is likely to be reflected in nanometer-scale measurements obtained by NSE, as well as in the resulting micrometer-scale distribution of vesicle sizes (52).

In summary, while a necessary step in many situations, the use of theoretical models for analyzing data from various sources often relies on assumptions that may be applicable under only certain scenarios. Such a dependency is circumvented by a direct method such as the Multi-Map approach.

The above discussion also raises another important concern, i.e. that inferring membrane structure purely from its experimentally determined dynamics is informative, but does not account for possible structural changes in the lipid molecules, or their preferential diffusion over time. Recently, Lessen et al. used a theoretical model to predict that mixed membranes are softer than their pure-lipid counterparts because of those two effects (56). Although this model may prove useful in further analyzing curvature-induced changes in lipid structure (Fig. 6), no significant redistribution of cholesterol is observed here for POPC/CHOL or DOPC/CHOL (Fig. 5C and D). We emphasize that this result is specific to the compositions studied and that cholesterol redistribution may indeed be observed in membranes that contain spontaneous phase-separated domains (25).

As noted, the bilayers considered in this study are symmetric, i.e. they have the same lipid composition in both leaflets. In future work, it will be of interest to examine the morphological properties of bilayers with asymmetric lipid compositions. Although many organelle membranes are symmetric, plasma membranes, for example, are known to be enriched in saturated acyl lipids in the outer leaflet, and correspondingly depleted in the cytoplasmic leaflet (57). This particular lipid make-up, together with a high cholesterol content (up to 40 mol%), suggests that the bending energetics of this membrane is dominated by the stiffness of its outer leaflet. A more definitive characterization, however, will require the determination of the concentrations of cholesterol in each leaflet, which remain unclear due to conflicting experimental results (58). Recent theoretical analyses have proposed that cholesterol is enriched in the outer leaflet, either because of its chemical affinity for saturated lipids (59), or because it helps to mitigate residual tension between the leaflets (60, 61). If so, such an imbalance would increase the already substantial stiffness of the outer leaflet. We anticipate that the methodology employed in this work, in synergy with experimental measurements, will help to quantify and explain how cholesterol asymmetry contributes to dictate the morphological energetics of lipid membranes.

We conclude this discussion by underscoring an interesting result specific to the shortest length scales considered in our simulations, namely $L < 100$ Å. At this length scale, we observe that the mechanism of curvature generation is unchanged upon the addition of cholesterol to a membrane and that there is little or no stiffening effect for *either* DOPC or POPC (Fig. 2). This is an important observation because it suggests that individual proteins in that membrane interact with a mechanically invariant environment even when the neighboring concentration of cholesterol is substantial. In other words, while cholesterol can impact membrane remodeling at scales comparable to lipid domains (25), it would not disrupt the activity of individual membrane proteins whose mechanisms entail local deformations of the membrane (5, 62). Quantitatively testing this hypothesis will prove essential for establishing how protein biochemistry dictates membrane morphology.

Methods

Systems, simulation specifications and trajectory analysis

Initial all-atom models of hydrated lipid bilayers were constructed by replicating pre-equilibrated configurations from an earlier study (26). The distance separating periodic images of each bilayer along the perpendicular to the midplane is about 70 Å; this water content is greater than that in multilamellar samples used for X-ray diffraction by more than 3-fold (28). Interatomic forces were represented via the CHARMM36 and TIP3P force fields (63, 64) using a 12-Å cutoff for Lennard-Jones forces and constraints for all covalent bonds involving hydrogen atoms. All simulations were performed with NAMD (65) at 300 K and 1 atm, using a 2-fs integration step. Coordinates were recorded every 20 ps and then used for analysis, which in most cases involved Python scripts based on MDAnalysis (66). Lipid orientation vectors $\mathbf{n}_i$ were defined as in earlier work (27, 43); that is, the vectors connect the midpoint between the phosphorus and glycerol C2 atoms in the lipid headgroup to the midpoint between the two terminal methyl carbons in the lipid chains. It has previously been observed (43) that using slightly different definitions of $\mathbf{n}$ (e.g. using only the phosphorous atom for the head group (42)) results in equivalent values of k_c and k_t from the same data. Lipid interdigitation was computed using MOSAICS (67), by measuring the mean of the index i of the carbon atoms that are within 6 Å from the terminal carbon of a chain from the opposing leaflet (with $i = 1$ indicating terminal carbons). Simulation snapshots were rendered with VMD (68).

Potentials-of-mean-force (PMF) of membrane bending

PMF profiles as a function of applied membrane curvature were calculated as described elsewhere (26). Briefly, one-dimensional density profiles of the lipid phosphate atoms were used to construct three-dimensional density maps, one for each leaflet, in a state of zero curvature. Sinusoidal deformations given by $\cos(2\pi x/L_x)$ were then applied to each leaflet's map to produce additional maps $\phi_k(\mathbf{x})$ that represent a series of curved bilayer states. The latter maps were then used to define the Multi-Map collective variable used to induce a deformation of the membrane (26). That is:

$$\xi(\mathbf{x}_1, \ldots \mathbf{x}_N) = \sum_{k=1}^{K} \xi_k \sum_{i=1}^{K} \phi_k(\mathbf{x}_i) \tag{8}$$

where $\mathbf{x}_i$ are coordinates of the phosphate atoms and ξ_k are constants quantifying the amount of curvature in each map. Note that ξ is directly proportional to $\mathrm{Re}(h_{\mathbf{q}_{(1,0)}})$ for a sinusoidal shape (26, 69). More complex shapes are also supported by the Multi-Map method (5, 26), but a sinusoid allows for simpler analytical expressions of the relevant vector fields (Eq. 3). Cholesterol molecules were not included in the definition of ξ, as they might migrate between leaflets, and their distribution was analyzed a posteriori.

To initialize the PMF calculations, values of ξ were derived from unbiased MD trajectories and collected into histograms with spacing ≈0.2 times the standard deviation of ξ. Random snapshots from each histogram bin were extracted from those trajectories and used to initialize umbrella-sampling windows (34). This choice improves statistical sampling compared to our previous computations with Multi-Map (26), where the windows were initialized from consecutive snapshots of a nonequilibrium simulation with a moving harmonic restraint on the Multi-Map variable. All the umbrella-sampling windows were simulated concurrently using NAMD and the Colvars module (70), with harmonic restraints on ξ of force constant 0.6 kcal/mol for ≈1 μs (Table 1).

Potentials-of-mean-force (PMF) were extracted using the WHAM (71) and FCAM (72) methods, with no significant differences between the two methods. To maximize the computing time dedicated to examine the cholesterol-enriched bilayers, the umbrella-sampling calculations for the 1800-lipid POPC and DOPC pure-lipid membranes used shorter sampling times than for the other systems, which were nevertheless sufficient to observe the convergence of their structural changes; the PMF curves in those two cases were however derived from unbiased histograms of ξ.

The structural properties of the 200-, 800-, and 1800-lipid bilayers were mapped onto two-dimensional grids of 25×25, 50×50 and 75×75 points, respectively, resulting in grid spacings of 3 Å or lower. Data were accumulated onto the respective grids by averaging over trajectory frames without any smoothing over grid points. To account for migration of cholesterol between leaflets during analysis, each cholesterol molecule was considered as part of a leaflet if its oxygen atom is within 10 Å from the phosphorus atom of any phospholipid molecule in that leaflet. Statistical correlations between different properties (for example, between the lipid orientation $\mathbf{n}$ and the normal vector $\mathbf{N}$) were estimated by linear regression across all grid points.

Acknowledgments

The authors thank Blue Waters team members James Phillips and William Kramer for their outstanding support. This manuscript was posted on a preprint (DOI: 10.1101/2023.02.02.525347).

Supplementary material

Supplementary material is available at *PNAS Nexus* online.

Funding

This research was supported by the Divisions of Intramural Research of the National Institute of Neurological Disorders and Stroke (G.F. and L.R.F., NS003139) and the National Heart, Lung and Blood Institute (J.D.F.-G.). Computer resources were in part provided by NIH, through the "Biowulf" supercomputer, and in part by the National Center for Supercomputing Applications, through the "Blue Waters" supercomputer (funded by National Science Foundation awards OCI-0725070 and ACI-1238993, the State of Illinois, and the National Geospatial-Intelligence Agency).

Data availability

Source code providing the Multi-Map enhanced-sampling simulation method is included in the Colvars library (https://colvars.github.io/) as well as in the standard version of NAMD 2.14 (https://www.ks.uiuc.edu/Research/namd/). Initial and final simulation snapshots are freely available from Zenodo (73); to download full trajectory data (40 TB), please contact the authors.

References

1 Bassereau P, *et al.* 2018. The 2018 biomembrane curvature and remodeling roadmap. *J Phys D: Appl Phys*. 51:343001.

2 Jarsch IK, Daste F, Gallop JL. 2016. Membrane curvature in cell biology: an integration of molecular mechanisms. *J Cell Biol*. 214:375–387.

3 Simunovic M, *et al.* 2016. How curvature-generating proteins build scaffolds on membrane nanotubes. *Proc Natl Acad Sci USA*. 113:11226–11231.

4 Nawrocki G, Im W, Sugita Y, Feig M. 2019. Clustering and dynamics of crowded proteins near membranes and their influence on membrane bending. *Proc Natl Acad Sci USA*. 116:24562–24567.

5 Zhou W, *et al.* 2019. Large-scale state-dependent membrane remodeling by a transporter protein. *eLife*. 8:e50576.

6 Guardia CM, *et al.* 2020. Structure of human ATG9a, the only transmembrane protein of the core autophagy machinery. *Cell Rep*. 31:107837.

7 Jensen LE, *et al.* 2022. Membrane curvature sensing and stabilization by the autophagic LC3 lipidation machinery. *Sci Adv*. 8: eadd1436.

8 Park YC, Reddy B, Bavi N, Perozo E, Faraldo-Gómez JD. 2023. State-specific morphological deformations of the lipid bilayer explain mechanosensitive gating of MscS ion channels. *eLife*. 12: e81445.

9 Khelashvili G, Harries D, Weinstein H. 2009. Modeling membrane deformations and lipid demixing upon protein-membrane interaction: the BAR dimer adsorption. *Biophys J*. 97:1626–1635.

10 Różycki B, Boura E, Hurley JH, Hummer G. 2012. Membrane-elasticity model of coatless vesicle budding induced by ESCRT complexes. *PLOS Comput Biol*. 8:e1002736.

11 Argudo D, Bethel NP, Marcoline FV, Wolgemuth CW, Grabe M. 2017. New continuum approaches for determining protein-induced membrane deformations. *Biophys J*. 112: 2159–2172.

12 Hassinger JE, Oster G, Drubin DG, Rangamani P. 2017. Design principles for robust vesiculation in clathrin-mediated endocytosis. *Proc Natl Acad Sci USA*. 114:E1118–E1127.

13 Guo SK, Sodt AJ, Johnson ME. 2022. Large self-assembled clathrin lattices spontaneously disassemble without sufficient adaptor proteins. *PLOS Comput Biol*. 18:e1009969.

14 Pollard TD, Earnshaw WC, Lippincott-Schwartz J, Johnson GT, editors. 2022. *Cell biology*. Cambridge (MA): Elsevier.

15 Chakraborty S, *et al.* 2020. How cholesterol stiffens unsaturated lipid membranes. *Proc Natl Acad Sci USA*. 117:21896–21905.

16 Nagle JF, *et al.* 2021. A needless but interesting controversy. *Proc Natl Acad Sci USA*. 118:e2025011118.

17 Ashkar R, *et al.* 2021. Reply to Nagle et al.: the universal stiffening effects of cholesterol on lipid membranes. *Proc Natl Acad Sci USA*. 118:e2102845118.

18 McConnell HM, Radhakrishnan A. 2003. Condensed complexes of cholesterol and phospholipids. *BBA-Biomembranes*. 1610: 159–173.

19 de Meyer F, Smit B. 2009. Effect of cholesterol on the structure of a phospholipid bilayer. *Proc Natl Acad Sci USA*. 106:3654–3658.

20 Henriksen J, *et al.* 2006. Universal behavior of membranes with sterols. *Biophys J*. 90:1639–1649.

21 Pan J, Mills TT, Tristram-Nagle S, Nagle JF. 2008. Cholesterol perturbs lipid bilayers nonuniversally. *Phys Rev Lett*. 100:198103.

22 Sorre B, *et al.* 2009. Curvature-driven lipid sorting needs proximity to a demixing point and is aided by proteins. *Proc Natl Acad Sci USA*. 106:5622–5626.

23 Tian A, Capraro BR, Esposito C, Baumgart T. 2009. Bending stiffness depends on curvature of ternary lipid mixture tubular membranes. *Biophys J*. 97:1636–1646.

24 Gracià RS, Bezlyepkina N, Knorr RL, Lipowsky R, Dimova R. 2010. Effect of cholesterol on the rigidity of saturated and unsaturated membranes: fluctuation and electrodeformation analysis of giant vesicles. *Soft Matter*. 6:1472–1482.

25 Baumgart T, *et al.* 2007. Large-scale fluid/fluid phase separation of proteins and lipids in giant plasma membrane vesicles. *Proc Natl Acad Sci USA*. 104:3165–3170.

26 Fiorin G, Marinelli F, Faraldo-Gómez JD. 2020. Direct derivation of free energies of membrane deformation and other solvent density variations from enhanced sampling molecular dynamics. *J Comput Chem*. 41:449–459.

27 Venable RM, Brown FLH, Pastor RW. 2015. Mechanical properties of lipid bilayers from molecular dynamics simulation. *Chem Phys Lipids*. 192:60–74.

28 Nagle JF. 2017. Experimentally determined tilt and bending moduli of single-component lipid bilayers. *Chem Phys Lipids*. 205: 18–24.

29 Mouritsen OG, Zuckermann MJ. 2004. What's so special about cholesterol? *Lipids*. 39:1101–1113.

30 Hung WC, Lee MT, Chen FY, Huang HW. 2007. The condensing effect of cholesterol in lipid bilayers. *Biophys J*. 92:3960–3967.

31 Ziblat R, Leiserowitz L, Addadi L. 2010. Crystalline domain structure and cholesterol crystal nucleation in single hydrated DPPC: cholesterol:POPC bilayers. *J Am Chem Soc*. 132:9920–9927.

32 Hamm M, Kozlov MM. 2000. Elastic energy of tilt and bending of fluid membranes. *Eur Phys J E*. 3:323–335.

33 May ER, Narang A, Kopelevich DI. 2007. Role of molecular tilt in thermal fluctuations of lipid membranes. *Phys Rev E*. 76:021913.

34 Torrie G, Valleau J. 1977. Nonphysical sampling distributions in monte carlo free-energy estimation: umbrella sampling. *J Comput Phys*. 23:187–199.

35 Watson MC, Brandt EG, Welch PM, Brown FLH. 2012. Determining biomembrane bending rigidities from simulations of modest size. *Phys Rev Lett*. 109:028102.

36 Jablin M, Akabori K, Nagle J. 2014. Experimental support for tilt-dependent theory of biomembrane mechanics. *Phys Rev Lett*. 113: 248102.

37 Canham P. 1970. The minimum energy of bending as a possible explanation of the biconcave shape of the human red blood cell. *J Theoret Biol*. 26:61–81.

38 Helfrich W. 1973. Elastic properties of lipid bilayers: theory and possible experiments. *Z Naturforsch C*. 28:693–703.

39 Goetz R, Gompper G, Lipowsky R. 1999. Mobility and elasticity of self-assembled membranes. *Phys Rev Lett*. 82:221–224.

40 Lindahl E, Edholm O. 2000. Mesoscopic undulations and thickness fluctuations in lipid bilayers from molecular dynamics simulations. *Biophys J*. 79:426–433.

41 Brannigan G, Brown FL. 2006. A consistent model for thermal fluctuations and protein-induced deformations in lipid bilayers. *Biophys J*. 90:1501–1520.

42 Ergüder MF, Deserno M. 2021. Identifying systematic errors in a power spectral analysis of simulated lipid membranes. *J Chem Phys*. 154:214103.

43 Levine ZA, *et al.* 2014. Determination of biomembrane bending moduli in fully atomistic simulations. *J Am Chem Soc*. 136: 13582–13585.

44 Terzi MM, Ergüder MF, Deserno M. 2019. A consistent quadratic curvature-tilt theory for fluid lipid membranes. *J Chem Phys*. 151:164108.

45 Beaven AH, Sapp K, Sodt AJ. 2023. Simulated dynamic cholesterol redistribution favors membrane fusion pore constriction. *Biophys J*. 122(11):2162–2175.

46 Molugu TR, Lee S, Brown MF. 2017. Concepts and methods of solid-state NMR spectroscopy applied to biomembranes. *Chem Rev*. 117:12087–12132.

47 Martinez-Seara H, *et al.* 2008. Interplay of unsaturated phospholipids and cholesterol in membranes: effect of the double-bond position. *Biophys J*. 95:3295–3305.
48 Rawicz W, Olbrich K, McIntosh T, Needham D, Evans E. 2000. Effect of chain length and unsaturation on elasticity of lipid bilayers. *Biophys J*. 79:328–339.
49 Bermúdez H, Hammer DA, Discher DE. 2003. Effect of bilayer thickness on membrane bending rigidity. *Langmuir*. 20:540–543.
50 Olsson N, Salem N. 1997. Molecular species analysis of phospholipids. *J Chromatogr B Biomed Appl*. 692:245–256.
51 Lippincott-Schwartz J, Phair RD. 2010. Lipids and cholesterol as regulators of traffic in the endomembrane system. *Annu Rev Biophys*. 39:559–578.
52 Karal MAS, *et al.* 2022. Effects of cholesterol on the size distribution and bending modulus of lipid vesicles. *PLoS One*. 17: e0263119.
53 Watson MC, Peng Y, Zheng Y, Brown FLH. 2011. The intermediate scattering function for lipid bilayer membranes: from nanometers to microns. *J Chem Phys*. 135:194701.
54 Doktorova M, Harries D, Khelashvili G. 2017. Determination of bending rigidity and tilt modulus of lipid membranes from real-space fluctuation analysis of molecular dynamics simulations. *Phys Chem Chem Phys*. 19:16806–16818.
55 Anthony AA, Sahin O, Yapici MK, Rogers D, Honerkamp-Smith AR. 2022. Systematic measurements of interleaflet friction in supported bilayers. *Biophys J*. 121:2981–2993.
56 Lessen HJ, Sapp KC, Beaven AH, Ashkar R, Sodt AJ. 2022. Molecular mechanisms of spontaneous curvature and softening in complex lipid bilayer mixtures. *Biophys J*. 121:3188–3199.
57 Lorent JH, *et al.* 2020. Plasma membranes are asymmetric in lipid unsaturation, packing and protein shape. *Nat Chem Biol*. 16: 644–652.
58 Steck TL, Lange Y. 2018. Transverse distribution of plasma membrane bilayer cholesterol: picking sides. *Traffic*. 19:750–760.
59 Allender D, Sodt A, Schick M. 2019. Cholesterol-dependent bending energy is important in cholesterol distribution of the plasma membrane. *Biophys J*. 116:2356–2366.
60 Hossein A, Deserno M. 2020. Spontaneous curvature, differential stress, and bending modulus of asymmetric lipid membranes. *Biophys J*. 118:624–642.
61 Varma M, Deserno M. 2022. Distribution of cholesterol in asymmetric membranes driven by composition and differential stress. *Biophys J*. 121:4001–4018.
62 Wang X, Boudker O. 2020. Large domain movements through the lipid bilayer mediate substrate release and inhibition of glutamate transporters. *eLife*. 9:e58417.
63 Klauda JB, *et al.* 2010. Update of the CHARMM all-atom additive force field for lipids: validation on six lipid types. *J Phys Chem B*. 114:7830–7843.
64 Jorgensen WL, Chandrasekhar J, Madura JD, Impey RW, Klein ML. 1983. Comparison of simple potential functions for simulating liquid water. *J Chem Phys*. 79:926–935.
65 Phillips JC, *et al.* 2020. Scalable molecular dynamics on CPU and GPU architectures with NAMD. *J Chem Phys*. 153:044130.
66 Michaud-Agrawal N, Denning EJ, Woolf TB, Beckstein O. 2011. MDAnalysis: a toolkit for the analysis of molecular dynamics simulations. *J Comput Chem*. 32:2319–2327.
67 Bernhardt N, Faraldo-Gómez JD. 2022. MOSAICS: a software suite for analysis of membrane structure and dynamics in simulated trajectories. *Biophys J*. 11:2023–2040.
68 Humphrey W, Dalke A, Schulten K. 1996. VMD: visual molecular dynamics. *J Mol Graph*. 14:33–38.
69 den Otter WK, Briels WJ. 2003. The bending rigidity of an amphiphilic bilayer from equilibrium and nonequilibrium molecular dynamics. *J Chem Phys*. 118:4712–4720.
70 Fiorin G, Klein ML, Hénin J. 2013. Using collective variables to drive molecular dynamics simulations. *Mol Phys*. 111:3345–3362.
71 Kumar S, Rosenberg JM, Bouzida D, Swendsen RH, Kollman PA. 1992. The weighted histogram analysis method for free-energy calculations on biomolecules. I. The method. *J Comput Chem*. 13:1011–1021.
72 Marinelli F, Faraldo-Gómez JD. 2021. Force-correction analysis method for derivation of multidimensional free-energy landscapes from adaptively biased replica simulations. *J Chem Theory Comput*. 17:6775–6788.
73 Fiorin G, Forrest LR, Faraldo-Gómez JD. 2023. Membrane free-energy landscapes derived from atomistic dynamics explain nonuniversal cholesterol-induced stiffening. Data files. https://doi.org/10.5281/ZENODO.7753728.